JOURNAL OF APPLIED PHYSICS **110**, 074305 (2011)

Thermal transport in double-wall carbon nanotubes using heat pulse

Liang Chen (陈良)[a] and Satish Kumar[a]
George W. Woodruff School of Mechanical Engineering, Georgia Institute of Technology, Atlanta, Georgia 30332, USA

(Received 18 May 2011; accepted 14 August 2011; published online 4 October 2011)

Multi-wall carbon nanotubes (MWCNTs) are outstanding materials for diverse applications such as electrodes, interconnects, or thermal management. Deep understanding of the underlying thermal transport mechanism in MWCNTs is crucial to engineer their thermal properties for a specific application. This paper investigates the interfacial thermal interaction in double-wall carbon nanotubes (DWCNTs) using molecular dynamics simulation and compares the transport in DWCNT with that in single-wall carbon nanotubes (SWCNTs). The present study is based on the application of intense heat pulse in the middle of the CNTs and analysis of wavelike responses of energy propagation as well as the kinetic energy corresponding to the velocity components in the radial, tangential, and longitudinal directions of CNTs. The analysis shows that the leading wave packets corresponding to the tangential and longitudinal components propagate ballistically along the tube, while the radial components show diffusive behavior with slow propagation speed. However, the radial components can efficiently transfer energy between tubes of DWCNTs while the fast moving longitudinal components and tangential components are weak in the interfacial energy transfer. An appropriate understanding of the energy exchange between different layers of tubes will pave the path of the future design of MWCNT based pellets and composites. © *2011 American Institute of Physics*. [doi:10.1063/1.3641970]

I. INTRODUCTION

Carbon nanotubes (CNTs) and CNT based composites are expected to have a great potential in a wide range of applications because of their exceptional thermal, electrical, and structural properties. The ultrahigh thermal conductivity of CNTs (~3000 W/mK) (Refs. 1 and 2) makes them promising candidates to be utilized in the thermal management applications such as thermal interface materials.[3,4] In these applications, CNTs need to be properly aligned and appropriately bonded to the substrate material in order to reduce the effect of contact thermal resistances at interfaces.[4,5] On the other hand, the thermal conductivity of CNT pellets is very low compared to a single isolated CNT (Ref. 6) as the thermal contact resistance between CNTs is very high, which dominates the conductive property of CNT networks.[7–9] High electrical conductivity but low thermal conductivity of CNT random network based composites and pellets have instigated research for these materials in energy harvesting applications.[10] These diverse behaviors and applications make exploration of the underlying transport mechanism in CNTs a very important research area. Recently, the metallic CNTs and their composites have been identified as advanced electrode materials in batteries, supercapacitors, fuel cells, and thermoelectric devices because of the low resistance, strong mechanical properties, and the superb current carrying capability.[11,12] The metallic CNTs have also been proposed as advanced interconnect materials for future integrated circuits to replace the copper (Cu) interconnects as Cu-interconnects may breakdown at high current densities due to electro-migration.[13–15] Since the chirality and other structural parameters cannot be well controlled in current synthesis technology, the additional purification process for metallic SWCNTs will inevitably increase the cost. On the contrary, multi-wall carbon nanotubes (MWCNTs), consisting of multiple concentric shells, are predominantly of metallic nature.[16] Thus, MWCNTs are attractive for these applications as they can be available at relatively low cost. The thermal transport characteristics of MWCNTs are of great importance as the performance of electrodes and interconnect using MWCNTs can be strongly affected by self-heating effects at high current densities. A detailed understanding of the interfacial interaction between layers of a MWNT and contribution of different layers in thermal transport can provide significant insights to engineer their thermal properties.

It is of fundamental interest to investigate the role of the phonon modes and phonon interactions in the study of bulk thermal conductivity of CNT array, pellet and composite, and the thermal boundary resistance between CNTs and substrate. Experimental and numerical studies have indicated that thermal transport is dominated by phonon contribution in both multi-wall CNTs (MWCNTs) and single-wall CNTs (SWCNTs) at all temperatures.[17] The long mean free path of phonons contribute to the high thermal conductivity of isolated long CNTs, while the phonon scattering from the tube ends, defects, and interfaces is thought to be responsible for the low thermal conductivity of short CNTs and bulk CNT materials.[18,19] Since phonon-phonon interactions have been included in a natural way, molecular dynamics simulation is a promising method to investigate the thermal transport in CNTs as well as the interfacial thermal transport between CNTs.[20–23] It has been revealed that the low frequency acoustic phonons play an important role in the thermal

[a]Electronic addresses: lchen64@gatech.edu or satish.kumar@me.gatech.edu.

transport of CNTs. The heat pulse analysis based on molecular dynamics (MD) simulations show that longitudinal acoustic (LA), twisting (TW) phonon modes, and second sound waves are excited in SWCNTs by the heat pulse and propagated as the leading wave packets with their own characteristic speed.[24] Moreover, the LA, TW phonon modes, and the second sound waves in the zig-zag type nanotubes can carry more energy than that in the armchair nanotube, which results in the higher thermal conductivity values for the zig-zag carbon SWCNTs compared with armchair SWCNTs at low temperatures.[25,26] Same heat pulse analysis on the double-wall carbon nanotubes (DWCNTs) indicates that the LA mode wave packets in DWCNTs carry five to seven times larger energy than that in the corresponding SWCNTs, which can be attributed to the presence of higher strain field in DWCNTs.[27] While the long-wavelength acoustic phonons are thought to be responsible for the high thermal conductivity of CNTs, modal analyses using wavelet transformations also show that the major contribution to the wavelike heat conduction in a SWNT with nanoscale length comes from the optical phonon modes with sufficient group velocity and probably with wave vector in the intermediate regime.[28]

MD simulations have been performed to estimate contact thermal resistances between CNTs and to investigate the role of different phonon modes.[29–31] A MD based study by Greaney and Grossman[31] for a system of two SWCNTs arranged parallel to each other show that energy exchanges efficiently between two nanotubes for modes in resonance and strongly depend on the strength of the intertube van der Waals interaction. Kumar and Murthy[29] investigated the interfacial thermal interaction between two CNTs placed in the crossed configuration. Their thermal pulse analysis showed that the coupling between the two tubes is very weak and may be dominated by slow-moving phonon modes with high energy. Recently, MD simulations demonstrate that the thermal resistance of carbon nanotube junctions can be significantly improved by modifying the molecular structure at the interface in order to enhance the matching of phonon spectra and phonon mode coupling.[32] Polymer wrapping is suggested to improve both the structural stability and interfacial thermal conductivity of carbon nanotube junctions. Most of the previous studies for exploring the interfacial thermal transport are focused on SWCNTs. The mechanism of thermal transport in MWCNTs, especially the energy exchange and phonon interaction between different layers of a MWNT is still not well understood and the focus of the present study.

In the present study, thermal energy transport between layers of DWCNTs is investigated in the framework of traveling wave packets and the thermal transport in DWCNT subjected to a heat pulse is compared against the thermal transport in SWCNTs in similar conditions. A strong heat pulse is generated in the middle of inner or outer layer of DWCNTs; the energy exchange and coupling of the vibration modes between these layers is analyzed through the kinetic energy corresponding to the velocities in the radial, tangential, and longitudinal directions. The wavelet analysis is then performed on these velocity components in order to elucidate the thermal interaction between layers of DWCNTS in the frequency domain. The goal is to understand the phonon interactions between layers of DWCNTs and identify the vibration modes that are strongly coupled between layers and which efficiently exchange energy.

The rest of this paper is organized as follows: In Sec. II, the details of MD simulations and wavelet analysis are explained. Results and discussion for thermal transport in SWNT and interfacial thermal interaction in DWNT using heat pulse and wavelet method are presented in Sec. III. Finally, Sec. IV concludes this paper.

II. METHODS

A. MD simulation details

The present MD simulations use the reactive empirical bond order (REBO) potential for C-C bond interaction and a truncated 12-6 type Lennard-Jones (LJ) potential for non-bonded van der Waals interactions between CNTs with fixed time step of 0.5 femtosecond (fs). The REBO potential is given by

$$U_{REBO} = \sum_i \sum_{i<j} \left[V_r(r_{ij}) - D_{ij} V_a(r_{ij}) \right],$$

where r_{ij} denotes the distance between atoms i and j, and V_r and V_a correspond to interatomic core-core repulsive and attractive interactions, respectively. Here, D_{ij} corresponds to a many-body empirical bond order term. The 12-6 type LJ potential for non bonded van der Waals interaction between individual carbon atoms is given as

$$U_{LJ} = 4\varepsilon\left[\left(\frac{\sigma}{r}\right)^{12} - \left(\frac{\sigma}{r}\right)^{6}\right].$$

Several different values of the energy and distance parameters in the LJ potential are considered for the interaction of C-C atoms in the CNT. The present study employs the parameterization used by Zhong and Lukes, with $\varepsilon = 4.41$ meV and $\sigma = 0.228$ nm.[30] The details of the MD code used for the present analysis may be found in Ref. 7. For CNTs with finite length, the boundary conditions have a significant effect on the thermal transport. In the present study, the two ends of the CNTs are set free, and the analysis is focused on the thermal transport before the heat pulses reach the ends. Simulations were also performed for CNTs with fixed ends, but no obvious difference was observed in the results before the heat pulses reach the ends.

The procedure of the MD simulation is as follows: First CNTs are quenched, using Berendsen thermostat,[33] to a very low temperature of 0.01 K for 900,000 to 1,100,000 time steps (450 ps–550 ps) as required to achieve thermal equilibrium at 0.01 K. Then, a strong heat pulse with 0.9 ps duration and a peak temperature of 800 K is applied to the ten slabs in the middle of the CNT of interest using the Berendsen thermostat. The heat pulse consists of a 0.1 ps rise time and a 0.8 ps duration with a constant temperature of 800 K. Finally, the thermostat are disconnected, and the system is kept at constant total energy for the rest of the simulations.

In our simulations, the kinetic temperature is related to the kinetic energy by

$$\frac{3}{2}nk_BT = \frac{1}{2}\sum_i^n m_i v_i^2,$$

where n is the number of atoms per slab, and m_i and v_i are the mass and velocity of each atom. k_B is the Boltzmann's constant. In order to investigate the contribution due to directional vibrations of atoms, kinetic energies corresponding to velocities in radial, tangential, and longitudinal directions are defined as radial component KE_r, tangential component KE_t, and longitudinal component KE_l. These are calculated using the radial, tangential, and longitudinal velocities, respectively, e.g., $KE_r = \frac{1}{2}\sum_i^n m_i v_{i,r}^2$, where $v_{i,r}$ is the radial component of the velocity. These components basically represent directional energy intensity in the corresponding direction. Besides, the kinetic energy of each slab is first time averaged over 200 time steps (0.1 ps) and then spatially averaged over ten slabs centered at the slab of interest to reduce the effect of statistical fluctuations. In order to examine the thermal transport along the CNTs, each CNT is divided in to 471 slabs per 100 nm along its axis. Each slab in (6, 0) and (12, 0) CNTs contains 12 and 24 atoms, respectively. The z-direction axis is along the longitudinal direction of CNTs, and its origin is located at the middle of the CNTs. The origins of x axis and y axis are at the center of a CNT cross section.

B. Wavelet analysis method

The wavelet transform (WT) is an analysis tool well suited for the study of transient processes that occur over finite spatial and temporal domains.[29] A WT uses generalized local functions known as wavelets that can be stretched and translated with a desired resolution in both the frequency and time domains.[34,35] Wavelets decompose a time series in the time-frequency space and are useful for identifying the evolution of dominant frequency modes with time. The WT of a signal ($s(t)$) is given as the convolution integral of $s(t)$ with ψ^*, where ψ^* is the complex conjugate of the mother wavelet function ψ,

$$W(b,a) = \frac{1}{a^{0.5}}\int \psi^*\left(\frac{t-b}{a}\right)s(t)dt,$$

where a and b are parameters that control dilation and translation, respectively. The parameter a is also known as the scale in the wavelet analysis. The power spectrum of a WT is defined as $|W|^2$. In the present study, we use Morlet wavelet as the mother wavelet that has the form of a plane wave with a Gaussian envelope and can be given by $\psi = e^{iwt} \times e^{-0.5|t|^2}$.

III. RESULTS AND DISCUSSION

As discussed in Sec. I, the understanding of the interfacial energy transfer and phonon interactions is very crucial to tune the transport properties of CNTs. In order to develop such an understanding of energy exchange and phonon interactions in DWCNTs, we present heat pulse analysis and thermal transport using MD simulations and wavelet methods on six different configurations of CNTs shown in Fig. 1. In order to reduce the background noise and effectively analyze the interfacial energy transfer, we keep the background temperature of CNTs low (~0.01 K) and apply intense heat pulse (~800 K) using Berendsen thermostat. We observe that the major trends of interfacial energy transfer remain same at smaller temperature differences and by using different thermostats. Heat pulse method to study the role of specific phonon modes in thermal transport of SWNTs through MD simulations has been employed before.[24,28] To illustrate the difference between the heat pulse propagation in SWCNTs and DWCNTs, simulations are first performed on SWCNTs (CNT I and CNT II in Fig. 1). Then, the heat pulse analysis is performed for two different configurations of DWCNTs with a 50 nm cut in the middle (CNT III and CNT IV in Fig. 1), and thermal energy transport between layers of DWCNTs is investigated in the framework of traveling wave packets. These two configurations with a cut in the middle help to avoid inter-layer energy transfer during the heating process and focus on the inter-layer thermal transport by the traveling heat wave packets. Next, we apply the heat pulse to two complete DWCNTs (CNT V and CNT VI in Fig. 1) to analyze the inter-layer energy transport during the heating process and compare them with two previous configurations with a cut in the middle. We compute kinetic energies corresponding to the vibrations in the radial, tangential, and longitudinal directions and analyze their propagation characteristics along the tube axis at different time instants. Following the heat pulse analysis, we perform wavelet analysis on all three velocity components of CNT atoms in order to analyze the evolution and propagation of different modes in the frequency space, which helps in illustrating phonon interactions between CNT layers. In particular, the acoustic phonon modes and radial breathing modes are of high interest to understand the thermal transport characteristics. The doubly degenerate transverse acoustic (TA) modes involve

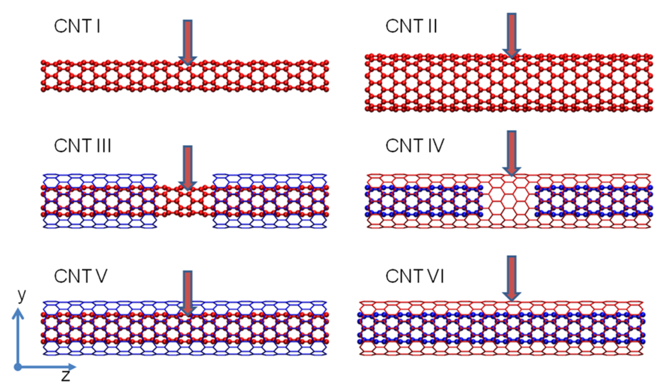

FIG. 1. (Color online) Schematic of CNTs in simulations (atoms of the outer layers are not shown for clarity). CNT I and CNT II are 200 nm long SWCNTs with chirality of (6, 0) and (12, 0), respectively; heat pulse is applied in the middle 10 slabs for these CNTs. CNT III is a 200 nm DWCNT with a 50 nm cut in the middle of the outer CNT. CNT IV is a 200 nm DWCNT with a 50 nm cut in the middle of the inner CNT. CNT V and CNT VI are 100 nm complete DWCNTs. The chirality of inner tube is (6, 0) and chirality of outer tube is (12, 0) for DWCNTs III to VI. The heat pulse is applied in the middle 10 slabs of the inner tube for CNT III and V and middle 10 slabs of the outer tube for CNT IV and VI.

the tangential and radial vibrations, and the longitudinal acoustic modes are due to the vibrations along the tube axis. The twisting modes (TW) are related to the rigid rotation around the tube axis. The radial breathing modes (RBM) are associated with the radial vibrations and correspond to the out of plane tangential acoustic mode in graphene sheet. Analysis of the propagation and frequency spectrum of the directional components of kinetic energy can provide information about the phonon modes excited by the heat pulse.

A. Heat pulse analysis of SWCNTs (CNT I and CNT II)

We first perform heat pulse analysis on SWCNTs of chiralities (6, 0) and (12, 0), which we refer as CNT I and CNT II. Kinetic energy profiles along tube axis of CNT II after heating are shown in Fig. 2. The characteristics of kinetic energy profiles of CNT I are similar to CNT II with differences only in magnitude. Kinetic energy profiles corresponding to three velocity components at different time instants along CNT II are shown in Fig. 2. During the heating process, 143.5 eV is added into the CNT I, while 198.6 eV is added into CNT II. Comparing the kinetic energy for three velocity components, we observe that the heat pulse excites strong radial components for both CNT I and CNT II, but they diffuse slowly around the middle of the tubes. Moreover, the magnitude of radial components in CNT I are smaller than that in CNT II after heating, but their leading wave front propagate toward the end with similar speed. The diffusive characteristics of radial components can be attributed to the phonon modes related to the radial vibrations, *e.g.*, RBM and other high frequency optical phonons with smaller group velocity than the high speed LA and TW modes. The frequency spectrum of the radial components shows that the leading wave fronts of the radial components may mainly involve TA modes. Referring to the dispersion curves in Ref. 26, the TA phonons have similar group velocity for CNTs with different diameters at small wave vectors, which may result in the similar propagation speed of the front radial components of CNT I and CNT II.

As shown in Fig. 2(c), the heat pulse excites tangential components with energy lower than the radial components but higher than the longitudinal components. The leading wave packets of tangential components propagate at the speed of about 13.1 km/s and 11.9 km/s in CNT I and CNT II, respectively, and can effectively spread energy along the tubes. This propagation speed falls into the speed range (11∼15 km/s) of TW phonons.[24,28] Reference 24 showed some high energy wave packets associated with second sound waves with similar speed (12.2∼12.9 km/s). But, the further observation of the atom vibrations shows rigid rotation around the tube axis and tube deflection during the heating process. Thus, the leading wave packets of the tangential components should be mainly contributed by TW and TA phonons excited by the heat pulse. The longitudinal components excited by the heat pulse are relatively small, but they propagate very fast along the tube with a speed of 20.9 km/s and 20.2 km/s in CNT I and CNT II, respectively, Fig. 2(d). This speed is in good agreement with speed of the sound waves associated with the longitudinal phonon modes (19.9 km/s to 21.7 km/s) in Ref. 24. By comparing Fig. 2(d) with Fig. 2(a), we observe that the leading wave packets in the total kinetic energy profiles are only contributed by this high speed longitudinal component.

B. Heat pulse analysis of DWCNTs with cut in the middle (CNT III and CNT IV)

In this section, we perform heat pulse analysis on two DWCNTs, one of which has a 50 nm cut in the outer layer (CNT III) and the other one has a 50 nm cut in the inner layer (CNT IV), Fig. 1. These two configurations have been chosen to avoid the inter-layer energy transfer during the heating process at the middle of the tube and thus focus on the inter-layer thermal transport due to the interaction of

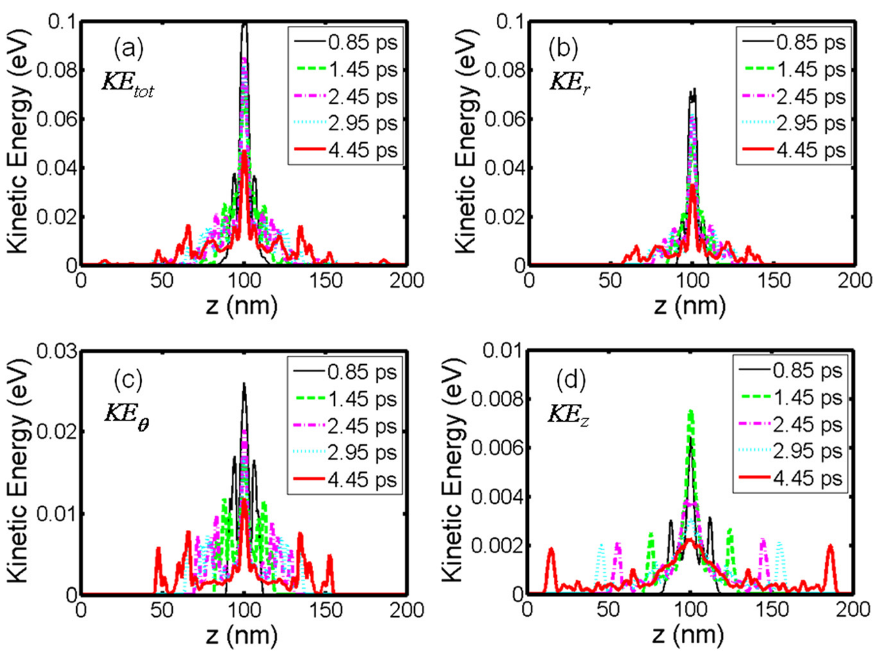

FIG. 2. (Color online) The location and shape of the heat pulse and kinetic energy corresponding to three velocity components at different time instants along CNT II: (a) Total kinetic energy (KE_{tot}); (b) radial component (KE_r); (c) tangential component (KE_θ); and (d) longitudinal component (KE_z).

propagating heat wave-packets of high speed, *e.g.*, tangential components and longitudinal components as indicated in CNT I and CNT II.

When the heat pulse is applied to the DWCNTs with a cut in the middle, 220.7 eV and 381.8 eV are added into CNT III and CNT IV, respectively. This energy is much higher than the energy added into the SWCNTs (CNT I and CNT II). This is because some strong tangential components are excited by the heat pulse, as shown in Fig. 3(d). Figures 3(a) and 3(b) show the energy transfer between the heated and unheated tubes after the heating. 6.8 eV energy is transferred from the inner tube to the outer tube in CNT III till the heat wave packets reached the end of the CNTs (4.5 ps), while a maximum of 4.9 eV is transferred from the outer tube to the inner tubes in CNT IV in 3.0 ps, Fig. 3. Comparing this energy transfer with the energy gained by the heated tube, we observe that the energy transfer between the heated tube and unheated tubes is very inefficient. Moreover, the energy transfer in CNT III from inner to outer tubes starts a little earlier than that in CNT IV from outer to inner tube because the leading wave packets (longitudinal waves) propagate a little faster in CNT III, as indicated by CNT I (20.9 km/s) and CNT II (20.2 km/s). From Fig. 3, it can be also observed that the energy transfer from the heated tube to unheated tube in CNT III increases monotonically until the heat wave packets reach the end of the tube. However, the energy transfer in CNT IV reaches the maximum at 3 ps after which energy is transferred back and forth between the heated and unheated tubes. This can be also attributed to the slight difference in the speed of longitudinal components. The faster propagating longitudinal components excited in the inner tube of CNT IV (corresponding to CNT I at 20.9 km/s) at beginning may interfere with the slower propagating longitudinal components of the outer heated tube (corresponding to CNT II at 20.2 km/s) and thereby counteracting further energy transfer across the interface.

In comparison to SWCNTs (see Fig. 2(b)), the heat pulse also excites strong radial components in CNT III and CNT IV, but the radial components of CNTs III and IV (see Fig. 3(c)) diffuse more slowly during the simulation period of 4.45 ps and are confined in the middle 50 nm. The magnitude of radial components in CNT III is smaller than that in CNT IV. Observations of atom vibrations of CNT III and CNT IV do not show any deflection perpendicular to the tube axis, which is related to TA phonons. The absence of TA phonon can be also confirmed by the absence of low frequency portion in frequency spectrum of radial velocity (see Fig. 5(b)). So the absence of TA phonons can lead to the lower propagation speed of radial components of CNT III and CNT IV. Moreover, unlike the SWCNTs, the excited tangential components are much stronger and carried the largest part of the kinetic energy. As shown in Fig. 3(d), the tangential components propagate with a speed of 12.5 km/s, which is approximately equal to the tangential wave speed in SWCNTs (CNT I and CNT II). Since the TA phonons may not be present for CNT III and CNT IV, the strong leading wave packets of tangential components are mainly contributed by TW phonons. The longitudinal components excited by the heat pulse in CNT III and CNT IV have little difference with CNT I and CNT II in terms of both magnitude and propagation speed, Fig. 3(e).

The kinetic energy in the unheated tubes is very small in comparison with kinetic energy in the heated tubes, Fig. 3(f). The kinetic temperature corresponding to the radial component and the tangential component in the unheated tubes are approximately close to the background temperature (0.01 K), and the longitudinal component is nearly equal to the total kinetic energy. It indicates that only longitudinal modes are excited in the unheated tubes during the energy transfer process, which might be the reason for the inefficient energy transfer between the tubes. This will be further discussed in the following wavelet analysis.

C. Heat pulse analysis of complete DWCNTs (CNT V and CNT VI)

As shown in the above heat pulse analysis for CNT III and CNT IV, the radial components diffuse slowly in the middle of the CNTs, and it does not reach the other layer region during our simulation period. Thus, in order to investigate the energy transfer through these slowly diffusing radial components, heat pulse analysis is performed on the complete DWCNTs. The heat pulse is applied in the middle

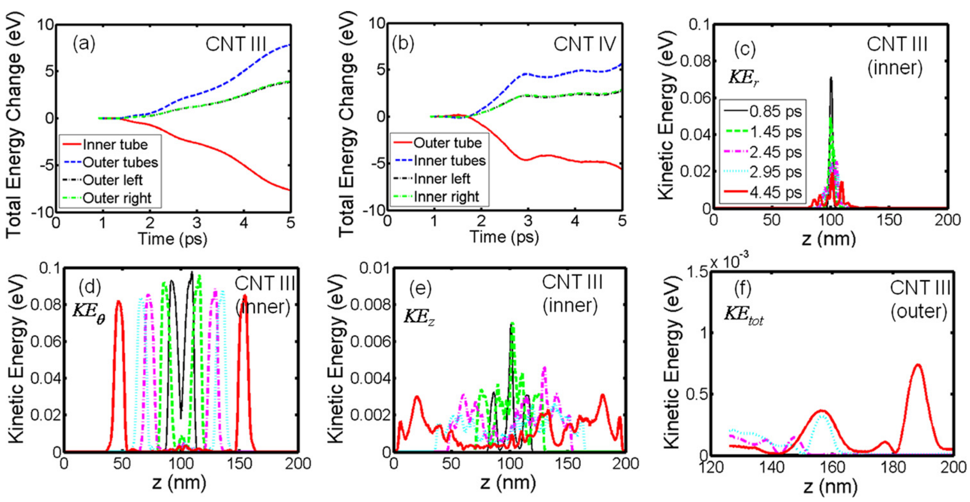

FIG. 3. (Color online) Total energy variation as a function of time with reference to total energy at t = 0.9 ps for (a) CNT III and (b) CNT IV. The heating process is completed at 0.9 ps. The location and shape of the heat pulse and kinetic energy corresponding to three velocity components at different time instants of CNT III: (c) radial component (KE_r) of heated (inner) tube; (d) tangential component (KE_θ) of heated (inner) tube; (e) longitudinal component (KE_z) of heated (inner) tube; and (f) total kinetic energy (KE_{tot}) profiles along unheated (outer) tube. (d)–(f) share the same legend with (c).

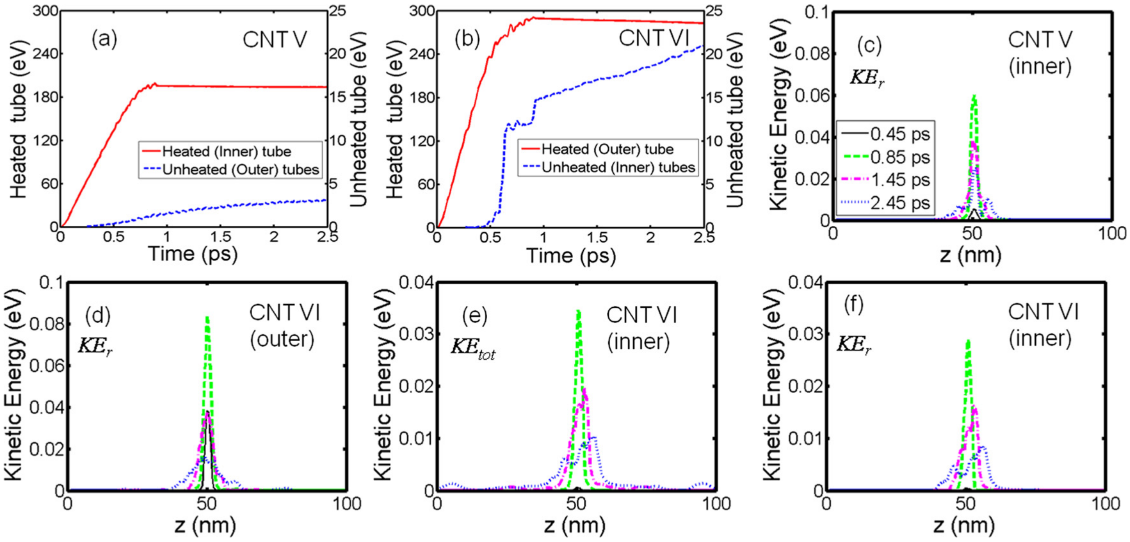

FIG. 4. (Color online) Total energy variation as a function of time with reference to total energy at t = 0.9 ps for (a) CNT V and (b) CNT VI. The heating process is completed at 0.9 ps. The location and shape of the heat pulse and kinetic energy corresponding to three velocity components at different time instants of CNT V and CNT VI: (c) radial component (KE_r) of heated (inner) tube of CNT V; (d) radial component (KE_r) of heated (outer) tube of CNT VI; (e) total kinetic energy (KE_{tot}) profiles of unheated (inner) tube of CNT VI; and (f) radial component (KE_r) of unheated tube (inner) of CNT VI. (d)–(f) share the same legend with (c).

of the inner layer and outer layer of CNT V and CNT VI, respectively, Fig. 1.

As shown in Figs. 4(a) and 4(b), the energies gained by the CNT V and CNT VI during the heating (0.9 ps) are 197.0 eV and 303.8 eV, respectively. Out of this total gained energy during the first 0.9 ps, 195.7 eV and 291.2 eV were directly gained by the heated tubes of CNT V and CNT VI, and 1.3 eV and 12.6 eV were transferred to the unheated tubes, respectively. It indicates that the energy transfer from inner tube to outer tube for CNT V during the heating period is negligible. Moreover, the energy transfer to the unheated tube is still very low during the first 0.5 ps, and it increases dramatically after 0.5 ps. The abrupt increase of energy transfer occurs again at 0.9 ps when the heating process ends. After the heating process, the energy transfer to the unheated tube of CNT V is also much smaller than that of CNT VI. The energy transfer between CNTs is dependent on the distribution of energy in different phonon modes. The excitation of radial phonon modes exhibit strong dependency on the CNT diameter, *i.e.*, under the applied heat pulse CNTs with different diameters may excite different distribution of radial phonon modes that participate differently in transmitting energy. The radial breathing modes of the outer tube of CNT VI have a lower frequency than that of the inner tube of CNT V. So, a larger population of radial breathing modes and other radial modes may be excited by the short heat pulse in the outer tube of CNT VI, which effectively transfers heat to inner CNT in comparison to the case V (∼ energy transfer from inner to outer tube). As shown in Fig. 4(d), the radial components of CNT VI are small before 0.5 ps. After 0.5 ps, the peak of radial components has increased up to 0.07eV, which lead to a large energy transfer to the unheated tube as shown in Figs. 4(b) and 4(e). However, at 0.55 ps, the peak of radial components of CNT V has kinetic energy below 0.02 V, which is much smaller than 0.07 eV of CNT VI. During the entire heating process (0.9 ps), the peak of radial components of CNT V is below 0.06 eV and energy transfer to the other tube is also low. Therefore, the larger magnitude of radial components of CNT VI indicates more radial modes are excited which leads to the large energy transfer in CNT VI. Besides, before 0.5 ps, most of the energy goes to the tangential components and generates strong leading wave packets involving twisting acoustic modes. As demonstrated by the simulation of CNT III and CNT IV, these strong leading wave packets do not transmit energy efficiently. So before 0.5 ps, there is little energy transferred to the unheated tube for CNT VI.

From Fig. 4(f), it can be observed that the radial components are dominant in unheated tubes of CNT VI and have similar profiles as the radial components in the heated tubes (Fig. 4(d)). This indicates that the radial components in the unheated tubes are excited by the corresponding radial components in the heated tube during the heating process, leading to large energy exchange. However, this cannot happen to DWCNTs with a cut in the middle (CNT IV) because the radial components only diffuse slowly in the middle of the heated tube and cannot reach the unheated tubes. Moreover, the tangential components and longitudinal components in the unheated tubes of CNT VI also gain a higher amount of energy (with magnitudes below 0.004 eV) than CNT III and CNT IV, but they are much smaller than the radial components. Diffusion like behavior in the middle of the CNTs is found for the three components of both CNT V and CNT VI. CNT III and CNT IV have shown ineffective interfacial energy transfer by the strong tangential components and weak longitudinal components excited by the heat pulse in the heated tube. So, we may expect that the tangential and longitudinal components in unheated tube of CNT V and CNT VI are excited by the radial components in the heated tube.

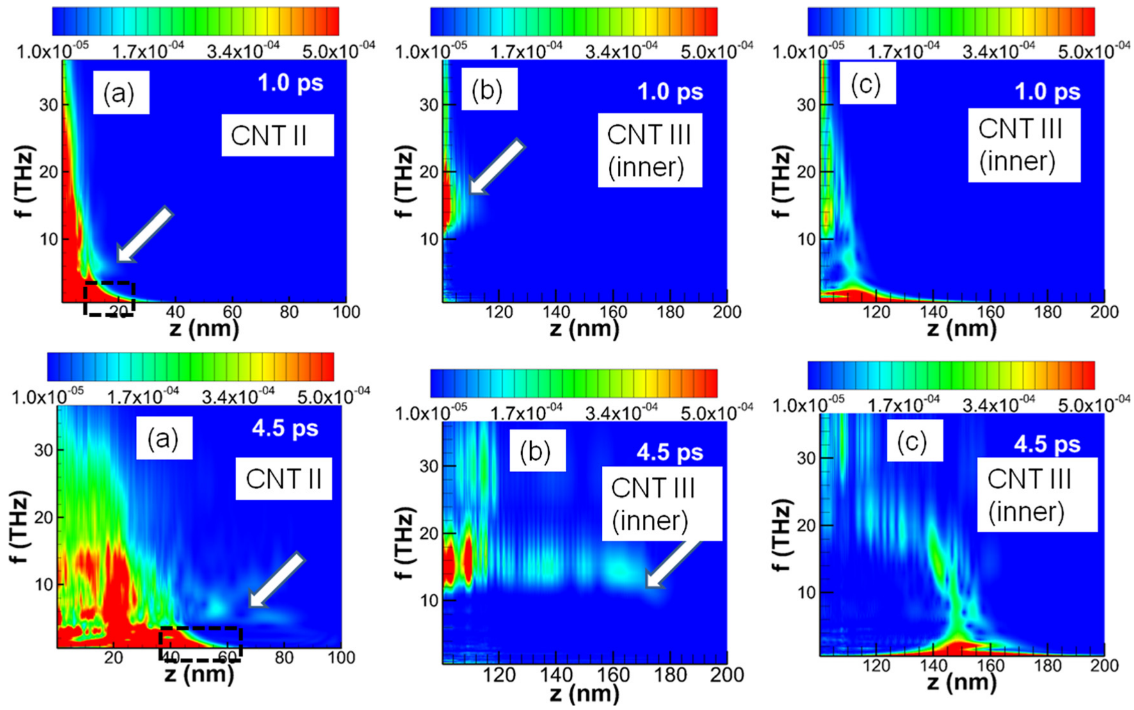

FIG. 5. (Color online) Frequency spectrum along the right half of the heated tubes of CNT II and CNT III at different time instants: (a) Radial component of CNT II; (b) radial component of heated tube of CNT III; and (c) tangential component of heated tube of CNT III.

D. Wavelet analysis

The power spectrum of the three velocity components of each atom in the nanotube is computed using the wavelet transform (WT). By summing the power spectrum over all the atoms of a slab, a one-dimensional projection of the temporal spectra along the nanotube axis is calculated. In this way, temporally evolving spectra of the three velocity components for the entire spatiotemporal field are obtained (Figs. 5–8).

As discussed in the heat pulse analysis of CNT I and CNT II, the leading radial components may be mainly composed of TA and RBM phonon modes. Figure 5(a) shows the

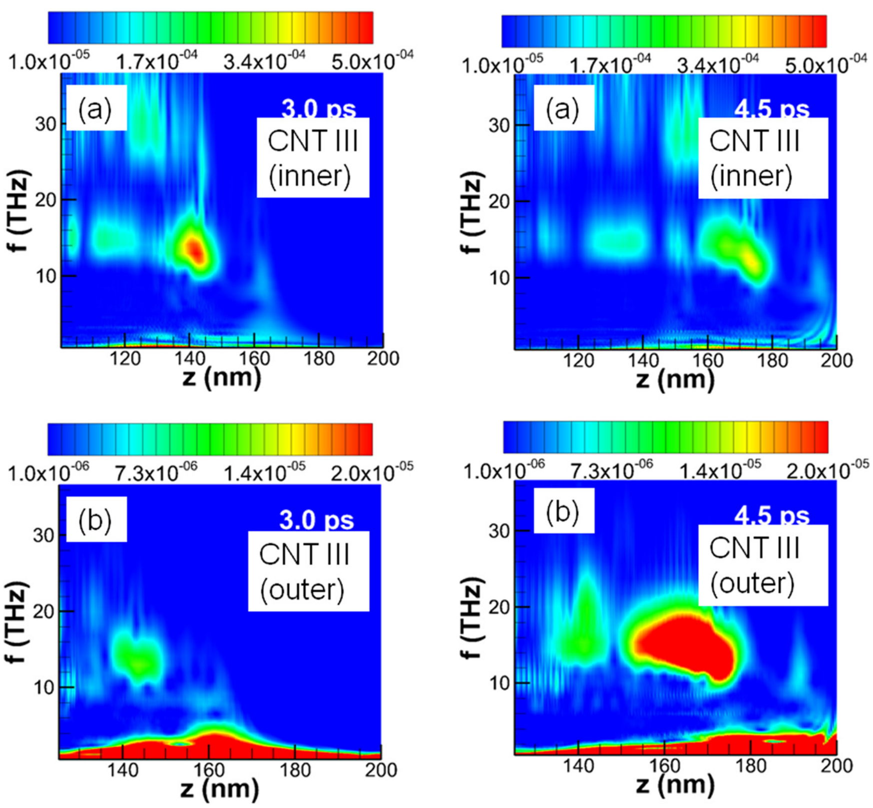

FIG. 6. (Color online) Frequency spectrum of the longitudinal velocity of CNT III at different time instants: (a) Longitudinal component of heated tube; (b) longitudinal component of unheated tube.

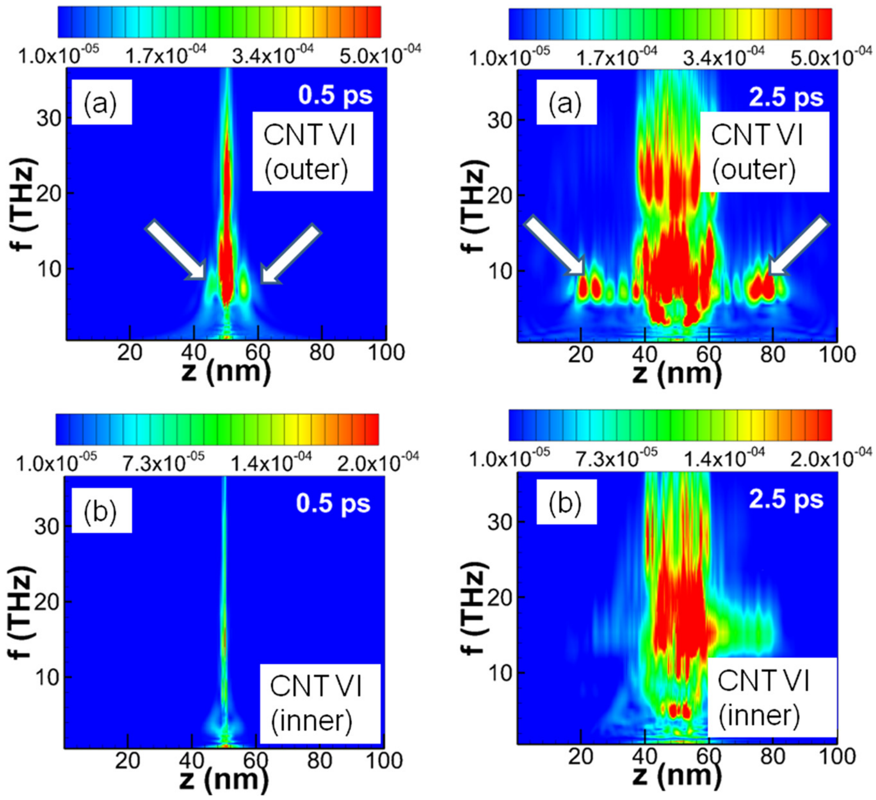

FIG. 7. (Color online) Frequency spectrum of the radial velocity of CNT VI at different time instants: (a) Heated (outer) tube; (b) unheated (inner) tube.

frequency spectrum along the right half of the heated tubes of CNT II at different time instants. It can be clearly observed that the leading radial components contain two frequency regions: the low frequency region with high power intensity (marked by dashed rectangular) and the high frequency region with low power intensity (marked by white arrow). The low frequency modes have a smaller group velocity than LA and TW modes and may be composed of TA modes. The high frequency modes are centered at 8 THz, which is same as the fast moving radial modes of heated

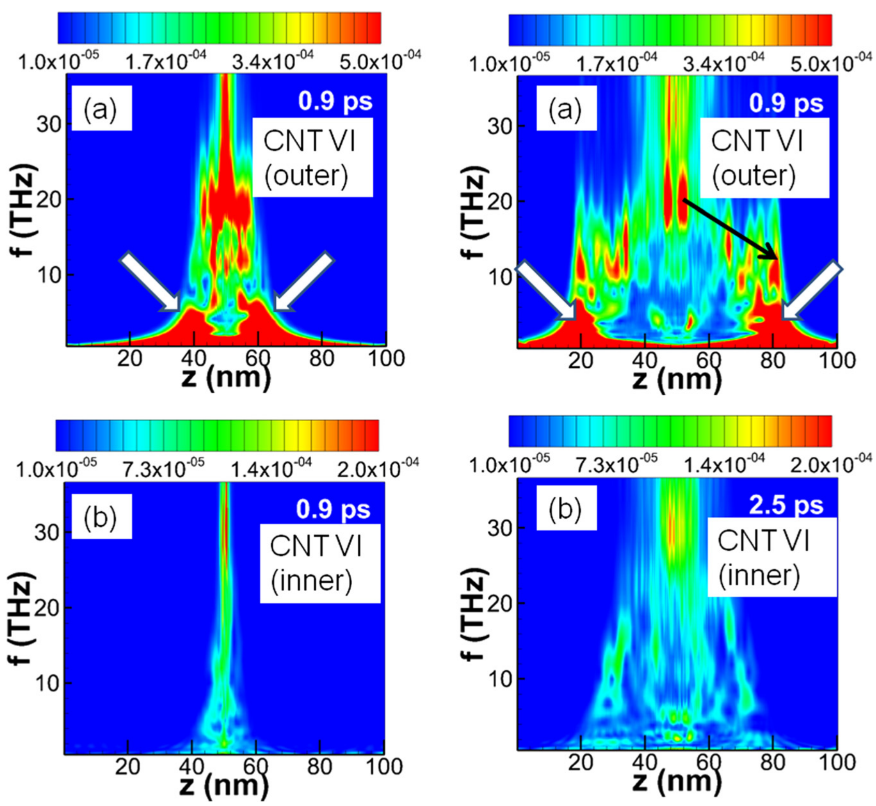

FIG. 8. (Color online) Frequency spectrum of the tangential velocity of CNT VI at different time instants: (a) Heated (outer) tube; (b) unheated (inner) tube.

tube of CNT VI (see Fig. 7(a)). This frequency is one half of the corresponding fast moving mode frequency (16 THz) of CNT III in Fig. 5(b). This is understandable because CNT II and the heated tube of CNT VI has a chirality of (12, 0), and its diameter is twice of the (6, 0) heated tube of CNT III. Reference 36 shows that the inverse dependence of the RBM frequency f on the tube diameter D, *i.e.*, $f \sim 1/D$. So, we may infer that the fast moving radial modes at high frequency are mainly contributed by RBM phonons.[36] Besides, frequency spectrum of radial components also shows much high frequency modes with high power intensity and smaller velocity, and they may be composed of optical phonon modes related to radial vibrations. As shown in Fig. 5(b), the radial components of the heated tube of CNT III are only composed of high frequency phonon modes (greater than 10 THz). The absence of low frequency modes (compared to Fig. 5(a)) indicates the TA modes are not excited by the heat pulse. This may be because the deflections of inner/outer tube perpendicular to the tube axis are restricted by the outer/inner tube for DWNTs (CNT III–CNT VI). Moreover, these high frequency radial components with high power intensity mainly diffuse in the middle, which is consistent with the heat pulse profiles shown in Fig. 3. As discussed in the heat pulse analysis of CNT III and IV, the leading wave packets of tangential components are mainly composed of TW modes. Figure 5(c) shows that these TW modes are concentrated in the low frequency region with a high propagating speed (see Fig. 3(d)).

Comparing Fig. 6(a) with Fig. 6(b), we find that the frequency and propagation of the longitudinal components in the unheated tubes match well with the frequency and propagation of the longitudinal components in the heated tube. This indicates that the longitudinal components in the unheated tubes may be excited by the corresponding longitudinal components in the heated tube. Together with the former discussion about heat pulse profiles in Fig. 3, we can conclude that the energy transfer between the tubes in CNT III and CNT IV is achieved by the longitudinal components. As mentioned previously, the kinetic temperature corresponding to the tangential components and radial components in the unheated tubes of CNT III and CNT IV are equal to the background temperature (0.01 K); this is further confirmed by our wavelet analysis showing that the tangential and radial components are not excited in the unheated tube. Although the leading wave packets of the tangential components have high energy intensity (Fig. 3(d) and Fig. 5(c)) in the heated tube, they do not excite any phonon modes in unheated tubes as they propagate.

As discussed in the previous section, the enhancement of the energy transfer between tubes in CNT VI may result from the radial components. This can be further supported by the frequency spectrum in Fig. 7. The frequency spectrums of the radial velocity of the heated tube and the unheated tubes in CNT VI are shown in Figs. 7(a) and 7(b). As shown in Fig. 7(a), the radial components are mainly composed of high frequency modes, which is similar to CNT III in Fig. 5(b). The fast moving modes of the radial component, the regions marked by the white arrows at the frequency of about 8 THz, is only a small portion. This is one half of the corresponding fast moving mode frequency (16 THz) of CNT III in Fig. 5(b). As discussed above, the fast moving modes of radial components are attributed to RBM phonons. Referring to Figs. 4(c) and 4(d), it can be observed that the energy intensity of these fast moving radial modes is very small. By comparing Figs. 7(a) and 7(b) and Fig. 4(f), we can observe that the fast moving radial modes in heated tube does not excite the corresponding part in the unheated tube. This can be attributed to their low energy intensity as well as the spectral mismatch between tubes with different diameters. On the contrary, the slow diffusing modes are excited in the unheated tube of CNT VI with frequency range similar to the slow diffusing modes in heated tube, Figs. 7(a) and 7(b). Thus, the slow diffusing radial components in the unheated tubes are excited by the slow diffusing radial components in the heated tube of CNT VI, considering that strong coupling and larger energy transfer can be expected between low speed phonon modes of similar frequencies.[31]

The tangential components of the heated tube have a different spectrum in comparison to the radial component, as shown in Fig. 8(a). The fast moving and low frequency tangential modes have very high intensity in the frequency spectrum of the tangential components. The evolution from high frequency modes to the low frequency modes can be also observed, as shown by the black arrow in Fig. 8(a). However, the fast moving and low frequency modes are not excited in the unheated tubes as shown in Fig. 8(b). Figure 8(b) also shows that the tangential velocity spectrum of the unheated tube mainly consists of the high frequency modes, and the low frequency spectrum is relatively weak. This indicates that typically high velocity phonon modes are inefficient in energy transfer.

IV. CONCLUSIONS

In summary, the present study investigates the heat pulse propagation in both SWCNTs and DWCNTs using MD and wavelet methods with a focus to analyze thermal coupling between the layers of DWNTS. In SWCNTs, the strong radial components excited by the heat pulse only diffuse around the middle of the tube; longitudinal components have the least energy content but they propagate effectively along the tubes with a speed of LA phonon modes. In DWCNTs, strong tangential components are excited by the heat pulse and can propagate effectively along the tubes with the propagation speed similar to the TW acoustic phonon modes. However, these fast moving tangential components are very ineffective in energy transfer between the tubes. The heat pulse and wavelet analysis show that the longitudinal components gain only a small part of the energy during the heating process and hence are not effective in energy exchange between tubes. We observe a large energy transfer from outer tube to inner tube of a DWCNT without any cut during the heating period; the transferred energy is primarily contained in the radial modes, which show that energy can be transferred effectively by the radial modes. A detailed study is further required to explore the coupling of specific phonon modes between the layers of MWCNTs.

[1]P. Kim, L. Shi, A. Majumdar, and P. L. McEuen, Phys. Rev. Lett. **87**, 215502 (2001).
[2]E. Pop, D. Mann, Q. Wang, K. Goodson, and H. J. Dai, Nano Lett. **6**, 96 (2006).
[3]B. A. Cola, X. F. Xu, T. S. Fisher, M. A. Capano, and P. B. Amama, Nanoscale Microscale Thermophys. Eng. **12**, 228 (2008).
[4]P. B. Amama, C. Lan, B. A. Cola, X. Xu, R. G. Reifenberger, and T. S. Fisher, J. Phys. Chem. C **112**, 19727 (2008).
[5]H. Huang, C. H. Liu, Y. Wu, and S. S. Fan, Adv. Mater. **17**, 1652 (2005).
[6]R. S. Prasher, X. J. Hu, Y. Chalopin, N. Mingo, K. Lofgreen, S. Volz, F. Cleri, and P. Keblinski, Phys. Rev. Lett. **102**, 105901 (2009).
[7]D. W. Brenner, O. A. Shenderova, J. A. Harrison, S. J. Stuart, B. Ni, and S. B. Sinnott, J. Phys.: Condens. Matter **14**, 783 (2002).
[8]M. B. Bryning, D. E. Milkie, M. F. Islam, J. M. Kikkawa, and A. G. Yodh, Appl. Phys. Lett. **87**, 161909 (2005).
[9]K. Chu, H. Guo, C. C. Jia, F. Z. Yin, X. M. Zhang, X. B. Liang, and H. Chen, Nanoscale Res. Lett. **5**, 868 (2010).
[10]C. Z. Meng, C. H. Liu, and S. S. Fan, Adv. Mater. **22**, 535 (2010).
[11]R. C. Hu, B. A. Cola, N. Haram, J. N. Barisci, S. Lee, S. Stoughton, G. Wallace, C. Too, M. Thomas, A. Gestos, M. E. dela Cruz, J. P. Ferraris, A. A. Zakhidov, and R. H. Baughman, Nano Lett. **10**, 838 (2010).
[12]R. K. Sharma, A. Karakoti, S. Seal, and L. Zhai, J. Power Sources **195**, 1256 (2010).
[13]J. C. Coiffic, M. Fayolle, S. Maitrejean, L. E. F. F. Torres, and H. Le Poche, Appl. Phys. Lett. **91**, 252107 (2007).
[14]J. C. Coiffic, D. Mariolle, N. Chevalier, S. Olivier, D. Lafond, M. Fayolle, S. Maitrejean, and H. Le Poche, Appl. Phys. Lett **92**, 223510 (2008).
[15]K. Rykaczewski, M. R. Henry, S. K. Kim, A. G. Fedorov, D. Kulkarni, S. Singamaneni, and V. V. Tsukruk, Nanotechnology **21**, 035202 (2010).
[16]M. P. Anantram and F. Leonard, Rep. Progress Phys. **69**, 507 (2006).
[17]M. S. Dresselhaus and P. C. Eklund, Adv. Phys. **49**, 705 (2000).
[18]N. Mingo and D. A. Broido, Nano Lett. **5**, 1221 (2005).
[19]D. J. Yang, Q. Zhang, G. Chen, S. F. Yoon, J. Ahn, S. G. Wang, Q. Zhou, Q. Wang, and J. Q. Li, Phys. Rev. B **66**, 165440 (2002).
[20]D. G. Cahill, W. K. Ford, K. E. Goodson, G. D. Mahan, A. Majumdar, H. J. Maris, R. Merlin, and S. R. Phillpot, J. Appl. Phys. **93**, 793 (2003).
[21]S. Maruyama, Physica B **323**, 193 (2002).
[22]S. Maruyama, Y. Igarashi, and Y. Shibuta, The 1st International Symposium on Micro & Nano Technology, Honolulu, Hawaii, USA, 2004.
[23]J. Shiomi and S. Maruyama, Jpn. J. Appl. Phys. **47**, 2005 (2008).
[24]M. A. Osman and D. Srivastava, Phys. Rev. B **72**, 125413 (2005).
[25]M. A. Osman and D. Srivastava, Nanotechnology **12**, 21 (2001).
[26]Y. Xiao, X. H. Yan, J. X. Cao, and J. W. Ding, J. Phys.: Condens. Matter **15**, L341 (2003).
[27]T. Kim, M. A. Osman, C. D. Richards, D. F. Bahr, and R. F. Richard, Phys. Rev. B **76**, 155424 (2007).
[28]J. Shiomi and S. Maruyama, Phys. Rev. B **73**, 205420 (2006).
[29]S. Kumar and J. Y. Murthy, J. Appl. Phys. **106**, 084302 (2009).
[30]H. L. Zhong and J. R. Lukes, Phys. Rev. B **74**, 125403 (2006).
[31]P. A. Greaney and J. C. Grossman, Phys. Rev. Lett. **98**, 125503 (2007).
[32]Z. Xu and M. J. Buehler, ACS Nano **3**, 2767 (2009).
[33]H. J. C. Berendsen, J. P. M. Postma, W. F. Vangunsteren, A. Dinola, and J. R. Haak, J. Chem. Phys. **81**, 3684 (1984).
[34]K. M. Lau and H. Weng, Bull. Am. Meteorol. Soc. **76**, 2391 (1995).
[35]C. Torrence and G. P. Compo, Bull. Am. Meteorol. Soc. **79**, 61 (1998).
[36]A. M. Rao, S. Bandow, E. Richter, and P. C. Eklund, Thin Solid Films **331**, 141 (1998).